Substrate-controlled allotropic phases and growth orientation of TiO2 epitaxial thin films

V. F. Silva, Valérie Bouquet, Stéphanie Députier, S. Boursicot, Sophie Ollivier, I.T. Weber, V. L. Silva, I. M. G. Santos, Maryline Guilloux-Viry, André Perrin

Journal of
Applied
Crystallography

ISSN 0021-8898

Received 21 May 2010
Accepted 13 October 2010

Substrate-controlled allotropic phases and growth orientation of TiO_2 epitaxial thin films

V. F. Silva,[a,b] V. Bouquet,[a]* S. Députier,[a] S. Boursicot,[a] S. Ollivier,[a] I. T. Weber,[c] V. L. Silva,[b] I. M. G. Santos,[d] M. Guilloux-Viry[a] and A. Perrin[a]

[a]Sciences Chimiques de Rennes, UMR 6226 CNRS/Université de Rennes 1, Campus de Beaulieu, 35042 Rennes Cedex, France, [b]LEAQ, Departamento de Engenharia Quimica, Universidade Federal de Pernambuco, CEP, Brazil, [c]Departamento de Química Fundamental, CCEN, Universidade Federal de Pernambuco, CEP, 50740-540 Recife, PE, Brazil, and [d]LACOM, Departamento de Química, Universidade Federal de Paraiba, Campus I, CEP, 58059-900 João Pessoa, PB, Brazil. Correspondence e-mail: valerie.bouquet@univ-rennes1.fr

TiO_2 thin films were grown by pulsed laser deposition on a wide variety of oxide single-crystal substrates and characterized in detail by four-circle X-ray diffraction. Films grown at 873 K on (100)-oriented $SrTiO_3$ and $LaAlO_3$ were (001)-oriented anatase, while on (100) MgO they were (100)-oriented. On (110) $SrTiO_3$ and MgO, (102) anatase was observed. On *M*-plane and *R*-plane sapphire, (001)- and (101)-oriented rutile films were obtained, respectively. On *C*-plane sapphire, the coexistence of (001) anatase, (112) anatase and (100) rutile was found; increasing the deposition temperature tended to increase the rutile proportion. Similarly, films grown at 973 K on (100) and (110) MgO showed the emergence, besides anatase, of (110) rutile. All these films were epitaxically grown, as shown by φ scans and/or pole figures, and the various observed orientations were explained on the basis of misfit considerations and interface arrangement.

1. Introduction

Titanium dioxide has attracted considerable attention because of its special properties, such as large energy gap, high refractive index and high dielectric constant. This oxide exists in three main crystallographic phases: rutile (tetragonal), anatase (tetragonal) and brookite (orthorhombic) (Banfield *et al.*, 1993). Anatase is known to be the low-temperature form of TiO_2 and it transforms irreversibly to the most stable rutile phase upon heating (Shannon & Pask, 1965), whereas brookite is rarer in nature and difficult to synthesize. TiO_2 is commonly used in optical devices, corrosion protective and self-cleaning coatings, sensors, and catalysts (Diedold, 2003; Walczak *et al.*, 2009). A better understanding of catalytic and photocatalytic processes is one of the main driving forces for TiO_2 surface investigation (Diedold, 2003).

To grow high-quality TiO_2 films various deposition methods have been used, such as atomic layer deposition (Aarik *et al.*, 2001; Heikkilä *et al.*, 2009; King *et al.*, 2008), chemical vapor deposition (Sobczyk-Guzenda *et al.*, 2009; Kim *et al.*, 2010; Sun *et al.*, 2008), sputtering (Singh *et al.*, 2008; Meng *et al.*, 2009; Heo *et al.*, 2005), electron beam evaporation (Lotnyk *et al.*, 2007) and pulsed laser deposition (PLD; Zhao & Lian, 2007; Walczak *et al.*, 2009; Yamamoto *et al.*, 2001). Crossing the published data, we can deduce that all these methods allowed the growth of epitaxial TiO_2 thin films on various substrates provided that a careful optimization of the deposition conditions was carried out. However, owing to the variety of the reported experimental conditions, it appears quite difficult to extract the specific contribution of the nature and orientation of the substrates.

The present investigation focuses then on the effects of substrate on epitaxial growth of TiO_2 thin films prepared by just one method, PLD, on a large selection of single-crystal substrates. The objective is to achieve accurate control of the allotropic variety and orientation of TiO_2 thin films, which will open the way to a comparative study of the surface effect on their behavior. In fact, it is expected that surface characteristics, morphology and crystallite orientations, inducing the development of active facets, would be of primary importance for applications such as photocatalysis and gas sensors (Lotnyk *et al.*, 2007). It is believed that knowledge of the surface properties on a fundamental level would help to improve material properties and device performance (Diedold, 2003). In particular, high-quality epitaxial anatase and rutile surfaces can be quite useful for understanding the photocatalytic mechanisms, independently of defect contributions (Yamamoto *et al.*, 2002).

2. Experimental

TiO_2 thin films were deposited by PLD on various substrates. Deposition was carried out using a KrF excimer laser (Tuilaser Excistar, pulse duration of 20 ns, $\lambda = 248$ nm). The laser beam,

incident at 45°, was focused in a standard vacuum chamber (background pressure of about 0.5 mPa) on a rotating target, whose surface was mechanically polished before each deposition run. The laser fluence was 2 J cm^{-2} with 2 Hz repetition rate. The distance between the target and the substrate was 42 mm. The deposition temperature was usually fixed at 873 K, but other temperatures (773–973 K) were also tested in specific examples. The oxygen pressure was 10 Pa and the deposition time was typically 30 min, leading to films about 100 nm thick.

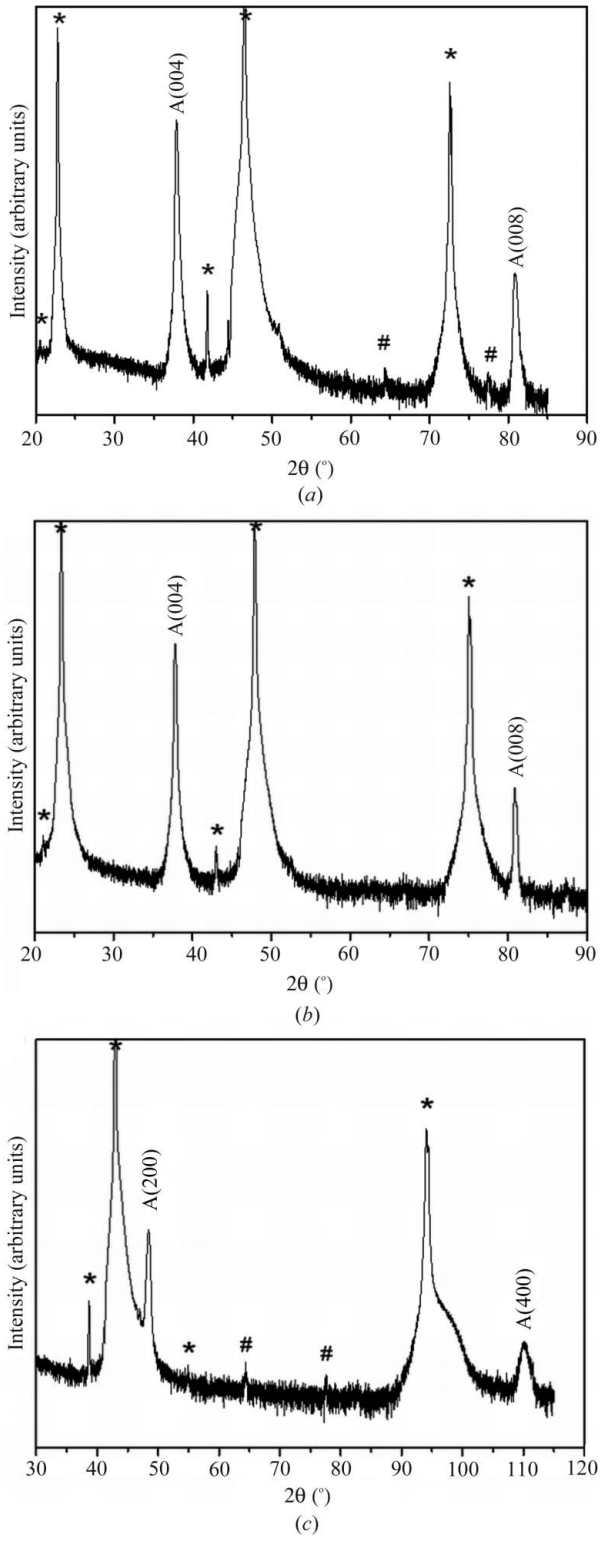

Figure 1
θ–2θ XRD patterns of TiO_2 thin films deposited at 873 K on (100)-oriented substrates: (*a*) STO, (*b*) LAO and (*c*) MgO. Diffraction peaks labeled A refer to the anatase phase. Peaks marked with a star (⋆) or a hash sign (#) are related to substrates and the sample holder, respectively. Note the logarithmic intensity scale.

A homemade target of TiO_2 rutile (99.8% purity) of 2.3 cm diameter was used, which was fabricated by sintering the cold-pressed TiO_2 powder pellet at 1373 K for 10 h in air. Single crystals of (100)-oriented $SrTiO_3$ (STO), MgO and $LaAlO_3$ (LAO), as well as (110)-oriented STO and MgO, and *R*-, *C*- and *M*-sapphire were used as substrates. Just before deposition, substrates were sonically cleaned in acetone and 2-propanol and air dried.

After deposition, samples were cooled under an oxygen pressure of about 3 kPa. No further *ex situ* annealing was used. All films appeared highly glossy and fully transparent, without cracks or macroscopic defects.

Standard θ–2θ X-ray diffraction (XRD) scans were performed with a two-circle Bruker D8 diffractometer using monochromated Cu $K\alpha_1$ radiation. Rocking curves, φ scans and asymmetric diffraction data were recorded with a four-circle Bruker D8 Advance diffractometer equipped with an Euler cradle and a Göbel mirror selecting a parallel beam of Cu $K\alpha$ radiation.

The surface morphology of the thin films was observed with a Jeol 6301-F field emission scanning electron microscope operated at low voltage (typically 9 kV) in order to limit charge effects and to achieve a high resolution without the need of surface metallization.

3. Results

In the following X-ray diffraction patterns, indexations refer to the tetragonal anatase phase [a = 3.7852, c = 9.5139 Å, space group $I4_1/amd$ (141), according to JCPDS 21-1272] or rutile phase [a = 4.5933, c = 2.9592 Å, space group $P4_2/mnm$ (136), according to JCPDS 21-1276].

3.1. TiO_2 film growth on (100)-oriented cubic substrates

Fig. 1 displays the θ–2θ XRD patterns of the films deposited at 873 K on various substrates. Figs. 1(*a*) and 1(*b*) refer to films grown on (100)STO and (100)LAO, respectively. They reveal only peaks due to (004) and (008) anatase, whereas Fig. 1(*c*) displays the (200) and (400) anatase diffraction peaks on (100)MgO. In summary, for the (100)-oriented substrates we obtained the anatase allotrope of TiO_2 alone. In order to evaluate the crystalline quality and in-plane orientation of these films, rocking curve and φ-scan analyses were performed.

Films deposited on the (100)STO substrate are oriented well out-of-plane (FWHM of the rocking curve $\Delta\omega = 0.84°$ for the 004 reflection) and epitaxied as shown by the φ scan displayed in Fig. 2(*a*). The four 90°-spaced peaks relative to the 103 reflection denote the fourfold symmetry of the (001)-

oriented film and arise at the same azimuth as the 110 peaks of the substrate. Then the epitaxial relations are the following:

$$(001)_{\text{anatase}}//(100)_{\text{STO}} \text{ and } \langle 100\rangle_{\text{anatase}}//\langle 001\rangle_{\text{STO}}. \quad (1)$$

The FWHM $\Delta\varphi = 1.3^\circ$ reflects a very good in-plane ordering in relation with a misfit of −3%. Even better results are obtained on LAO substrates, as $\Delta\omega = 0.24^\circ$ and $\Delta\varphi = 0.39^\circ$ (not shown), thanks to a misfit of only −0.01%. The epitaxial relations are the same as above.

Films grown on (100)MgO are, in contrast, (100)-oriented while exhibiting also well defined out-of-plane ordering ($\Delta\omega = 1.54^\circ$). The φ scan (Fig. 2*b*) displays four peaks denoting some in-plane ordering, but their width is as large as $\Delta\varphi = 18^\circ$, meaning strong in-plane dispersion. The latter could be related both to a large misfit {−10 and +13% for *a* and *c* [referring to $(c/2)_{\text{anatase}}$] anatase unit-cell constants, respectively} and to the competition between two in-plane orientations, defined by $[010]_{\text{anatase}}//[001]_{\text{MgO}}$ and $[001]_{\text{anatase}}//[001]_{\text{MgO}}$, respectively. The coexistence of these two orientations is reflected by the observation of four peaks, while the (100) plane has only twofold symmetry. This coexistence agrees with a previous report by Hesse & Bethge (1981) in the case of samples grown between 773 and 973 K by electron beam evaporation.

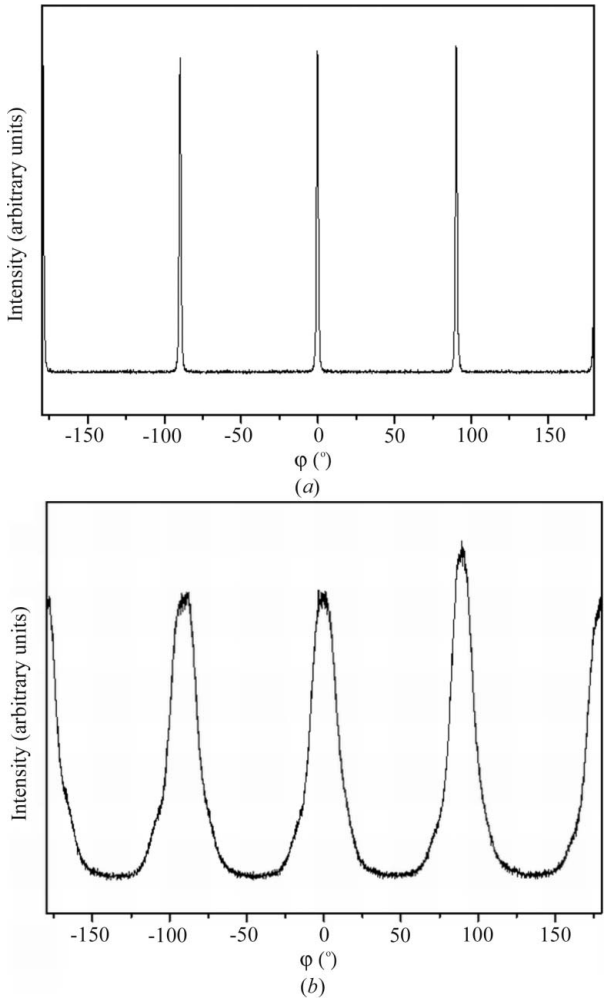

Figure 2
φ-scan XRD patterns of TiO_2 thin films deposited at 873 K on (100)-oriented substrates: (*a*) STO and (*b*) MgO. The probed reflection is $\{101\}_{\text{anatase}}$ in the two examples.

Aiming to eventually improve the in-plane ordering, a sample was deposited at higher temperature, namely 973 K, on (100)MgO. This resulted in the growth, besides the previous (100)-oriented anatase, of (110) rutile crystallites (not shown). From φ-scan analysis it appeared that the anatase in-plane ordering was not improved ($\Delta\varphi = 20^\circ$), while the rutile crystallites were epitaxied ($\Delta\varphi = 4^\circ$) with the following in-plane relationships:

$$[001]_{\text{rutile}}//[0\bar{1}1]_{\text{MgO}} \text{ and then } [110]_{\text{rutile}}//[011]_{\text{MgO}}, \quad (2)$$

meaning that the (110) rutile plane is rotated 45° with respect to the MgO basal square, and the misfits are then −0.4 and 9% along the rutile [001] and [110] vectors, respectively.

In contrast, decreasing the deposition temperature down to 773 K resulted in the growth of pure (100)-oriented anatase with a slightly better degree of in-plane ordering ($\Delta\varphi = 12^\circ$, compared to $\Delta\varphi = 18^\circ$ obtained at 873 K).

Fig. 3 displays field emission scanning electron microscopy (FE-SEM) secondary electron images for TiO_2 films grown on (100)-oriented substrates at 873 K. The samples present homogeneous and crack-free surfaces. However, the surface morphologies are influenced by the nature of the substrate. The films deposited on (100)MgO, which are not well ordered according to XRD, appear quite rough (Fig. 3*c*), while on (100)STO the TiO_2 film appears very smooth despite some accidental outgrowths (Fig. 3*a*). The film deposited on (100)LAO clearly shows well organized square-shaped crystallites (Fig. 3*b*), the edges of which are aligned with the unit-cell vectors of the substrate surface; these crystallites appear to be self-organized along the striations related to twin boundaries of the substrate, suggesting that such defects play a role in the nucleation stage.

3.2. TiO_2 film growth on (110)-oriented cubic substrates

Films were deposited on (110)STO substrates at 873 K and on (110)MgO at 773, 873 and 973 K. The θ–2θ XRD pattern of the film obtained at 873 K on (110)STO (Fig. 4*a*) shows only one peak at $2\theta = 62.72^\circ$ ($\Delta\omega = 0.96^\circ$), which can correspond either to (002) rutile, with a displacement of $2\theta = 0.02^\circ$, or to (204) anatase, with a displacement of $2\theta = 0.03^\circ$ with respect to JCPDS reference files. In order to resolve this uncertainty, oblique planes with respect to the basal one were probed. Indeed, in the first hypothesis the (101) plane of rutile would diffract at about $2\theta = 36.08^\circ$ and χ (the angle between the basal plane and the probed one) = 32.82°, while in the second case the 004 peak of anatase is expected at $2\theta = 37.80^\circ$ and $\chi = 51.49^\circ$. No diffraction was found in the first configuration, whereas a strong peak appeared for the second one, clearly evidencing that this film is crystallized in the anatase allotrope. The full φ-scan pattern taken for the (004) reflection (Fig. 4*b*) shows that the film is epitaxied, with two 180°-spaced peaks

aligned with the (200) peaks of the substrate, evidencing the following relationships:

$$(102)_{\text{anatase}}//(110)_{\text{STO}} \text{ with } \langle 100\rangle_{\text{anatase}}//[001]_{\text{STO}} \text{ and } [20\bar{1}]_{\text{anatase}}//[1\bar{1}0]_{\text{STO}}. \quad (3)$$

Because the (102) plane of anatase has no true twofold symmetry, only one peak would have been expected. The second one arises from crystallites having their $(\bar{1}02)$ plane, strictly identical to the previous (102) plane, parallel to the (110) substrate surface (this twinning mechanism can also be understood as a 180° in-plane rotation of the crystallites, which is strictly equivalent): then the two peaks are 180°-spaced. The $\Delta\varphi$ value of 2.3° reflects good in-plane orientation; indeed the misfit between the substrate surface and the film interfacial plane is about −3% along the [010] direction and 10% along the $[20\bar{1}]$ direction of the film.

The θ–2θ XRD pattern of the film obtained at 873 K on (110)MgO did not exhibit any peak in addition to the substrate peaks (not shown), making it impossible to obtain any information about the crystallinity and orientation. Then, complete pole figures were recorded for the (110) rutile and (101) anatase diffraction planes. No peak was observed in the first case, while eight discrete peaks appeared in the second case (Fig. 5), demonstrating epitaxically grown anatase. A model built from the *CaRine Crystallography* software (Bourdias & Monceau, 1998) clearly shows that the film is (102)-oriented anatase. Four peaks are directly explained by the model, while the other four are related to a twinning

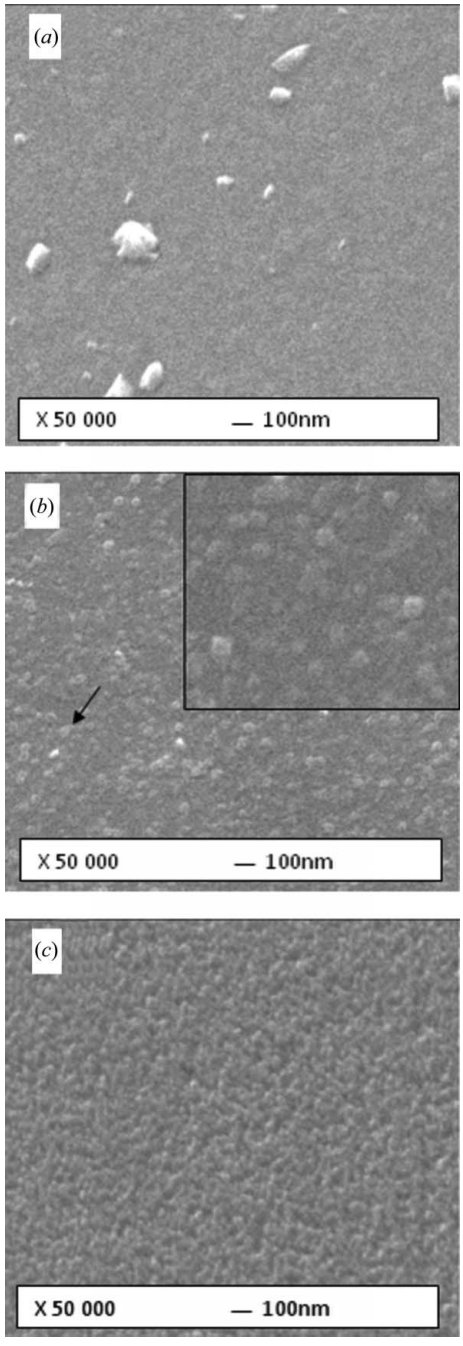

Figure 3
FE-SEM images of TiO_2 thin films deposited at 873 K on (100)-oriented substrates: (*a*) STO, (*b*) LaO and (*c*) MgO. The arrow on the image relative to LAO materializes the twin boundaries of the substrate. Inset is an image of the same film at higher magnification (×100 000)

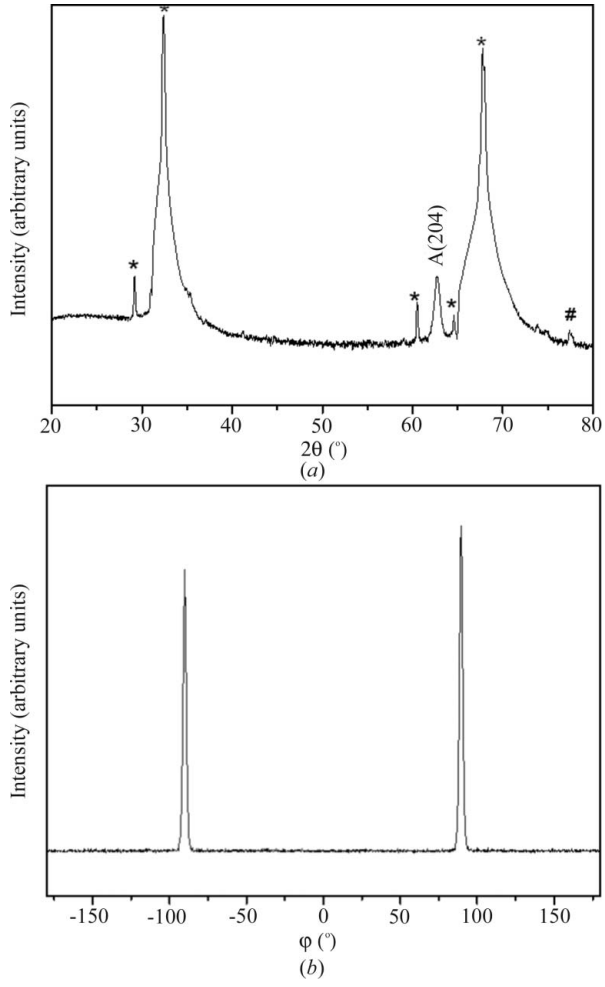

Figure 4
XRD patterns of the film deposited at 873 K on (110)STO: (*a*) θ–2θ XRD pattern [peaks marked with a star (⋆) or a hash sign (#) are related to substrates and the sample holder, respectively; note the logarithmic intensity scale] and (*b*) φ scan obtained for the probed plane $(004)_{\text{anatase}}$.

mechanism, as mentioned above. The epitaxial relations are the same as above on (110)STO,

$$(102)_{\text{anatase}}//(110)_{\text{MgO}} \text{ with } \langle 100\rangle_{\text{anatase}}//[001]_{\text{MgO}} \text{ and } [20\bar{1}]_{\text{anatase}}//[1\bar{1}0]_{\text{MgO}}, \quad (4)$$

with misfit values of −10 and 2%, instead of −3 and 10% for (110)STO, along the anatase [010] and $[20\bar{1}]$ directions, respectively. No diffraction was observed on a standard θ–2θ scan because the anatase 102 reflection is forbidden and the 204 reflection is fully masked by the 220 substrate reflection.

The θ–2θ XRD pattern of the film obtained at 973 K on (110)MgO (Fig. 6) shows two peaks located at 2θ = 27.43 and 56.52°, unambiguously assigned to (110) and (220) rutile. The rocking curve gives large values of $\Delta\omega$ (6.88°), meaning very important out-of-plane dispersion. However, the φ scan obtained for the (200) reflection has clearly shown that the film was epitaxically grown, with quite good in-plane orientation ($\Delta\varphi$ = 2.6°), a surprising result if one refers to the large mosaicity of this film. This φ scan exhibited, as expected, two peaks, 180°-spaced, reflecting the twofold symmetry of both the substrate and the film. As these peaks are 90°-shifted with respect to the azimuth of the substrate {200} reflections, the epitaxial relationships are

$$(110)_{\text{rutile}}//(110)_{\text{MgO}} \text{ with } [001]_{\text{rutile}}//[1\bar{1}0]_{\text{MgO}} \text{ and then } [1\bar{1}0]_{\text{rutile}}//[001]_{\text{MgO}}. \quad (5)$$

In these conditions, $2c_{\text{rutile}}$ fits closely the $[1\bar{1}0]$ vector of MgO (misfit = −0.5%) and, in the other direction, $2 \times [1\bar{1}0]_{\text{rutile}}$ compares very well with $3 \times [001]_{\text{MgO}}$ (misfit = 3%). Then this orientation could be stabilized, at least to some extent, by a near coincidence site lattice (NCSL) mechanism (Kwang *et al.*, 1980).

An additional set of φ scans, relative to the 004 anatase peak, revealed again the presence of the (102) anatase orientation, undetectable from θ–2θ scans, as previously mentioned. The volume ratio of the (102) anatase to the (110) rutile orientations was roughly estimated to be about 0.9, from the relative intensities of the 004 anatase and the 200 rutile peaks, integrated over $\Delta\omega$ and $\Delta\varphi$ and corrected for powder relative intensities normalized to corundum and multiplicities.

It is worth noting that some samples deposited at 973 K exhibited a very weak and broad peak at 29.95°, in contrast to films grown at 873 K. This peak could be attributed to either the 121 reflection of brookite or the 220 reflection of Mg_2TiO_4 (cubic, a = 8.4409 Å). From φ-scan experiments, no oblique plane of brookite was observed, while the 311 and 111 reflections of Mg_2TiO_4 were clearly detected. This interfacial phase is then also epitaxically grown, and grows cube-on-cube on MgO. The misfit with respect to the substrate is only 0.2%; then the misfit between TiO_2 and MgO or Mg_2TiO_4 is essentially the same. This result fully confirms the observation of a topotactic growth of Mg_2TiO_4 on MgO evidenced by Hesse & Bethge (1981) at temperatures above 1073 K, on the basis of transmission electron microscopy.

For a lower deposition temperature (773 K), the film appeared to be (110)-oriented anatase, with a quite large out-of-plane distribution ($\Delta\omega$ = 5°) but standard in-plane ordering ($\Delta\varphi$ = 3.5°). From φ scans recorded for the 200 reflection, the epitaxial relations are

$$(110)_{\text{anatase}}//(110)_{\text{MgO}} \text{ with } [001]_{\text{anatase}}//[001]_{\text{MgO}} \text{ and } [1\bar{1}0]_{\text{anatase}}//[1\bar{1}0]_{\text{MgO}}. \quad (6)$$

The misfit values are 13% (for two MgO unit cells fitting one anatase unit cell along their c axes) and −5%, respectively. However, the film contains again some epitaxial (102)-oriented anatase crystallites, as evidenced by the φ scan taken around the 004 reflection of anatase. These (102)-oriented crystallites represent roughly 30% of the total volume as evaluated from the intensities of the 004 and 200 anatase peaks, integrated over $\Delta\omega$ and $\Delta\varphi$ and corrected for multiplicities.

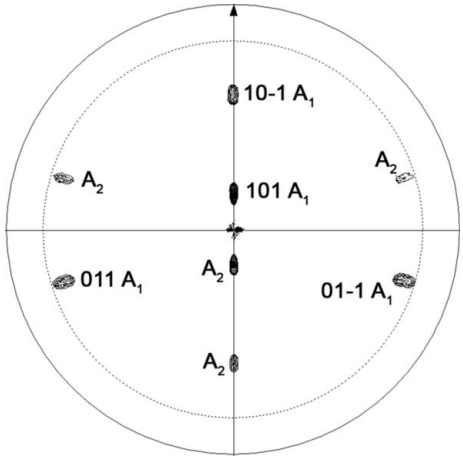

Figure 5
Pole figure obtained for the 101 peaks of the (204)-oriented anatase film deposited at 873 K on (110)MgO; one variant of the twin is fully indexed (A1); the indexations of the second variant (A2), not shown for clarity, are deduced with respect to the horizontal symmetry plane.

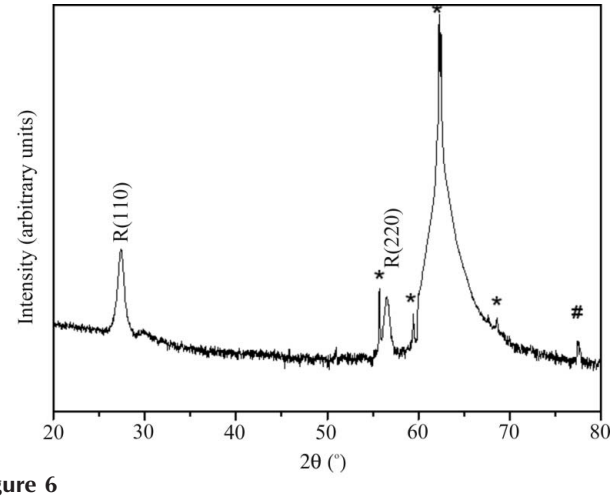

Figure 6
θ–2θ XRD pattern of the film deposited at 973 K on (110)MgO. Diffraction peaks labeled R refer to the rutile phase. Peaks marked with a star (⋆) or a hash sign (#) are related to substrates and the sample holder, respectively. Note the logarithmic intensity scale.

To summarize, in the case of these different (110)-oriented substrates, the growth of (102) anatase on (110)STO corresponds to reasonable misfits, while the hypothetical growth of (110) rutile would give very important misfits (+7 and −17% along the two in-plane directions), a reason to stabilize the former one. On (110)MgO, the (110) rutile presents a very good fit (−0.5 and 3%), while the alternative (102) anatase growth leads to values of −2 and 10%, favoring strongly the rutile allotrope when the thermal energy is enough to induce the phase transition.

Fig. 7 displays SEM secondary electron images for TiO_2 films on (110)STO and (110)MgO substrates. Both films present a very homogeneous and smooth surface with very small crystallites. There is no remarkable difference related to film orientation.

3.3. TiO_2 film growth on sapphire single-crystal substrates

Films were deposited on *M*-plane ($10\bar{1}0$), *C*-plane (0001) and *R*-plane ($10\bar{1}2$) sapphire substrates, in most cases at 873 and 973 K. For all substrates, increasing the deposition temperature results in an increase of crystallinity. Fig. 8 shows as an example the θ–2θ XRD patterns of films grown at 973 K.

3.3.1. TiO_2 films on *M*-plane sapphire. The θ–2θ scan (Fig. 8*a*) shows only one peak ($2\theta = 62.96^\circ$, $\Delta\omega = 0.82^\circ$), which could be attributed either to the 002 reflection of the rutile variant or the 204 reflection of the anatase one, as in the case of the film grown on (110)STO. In the φ-scan mode, a strong peak was observed near $2\theta = 36.08^\circ$ and $\chi = 32.82^\circ$; thus the film is clearly (001) rutile (refer to §3.2). The full φ-scan

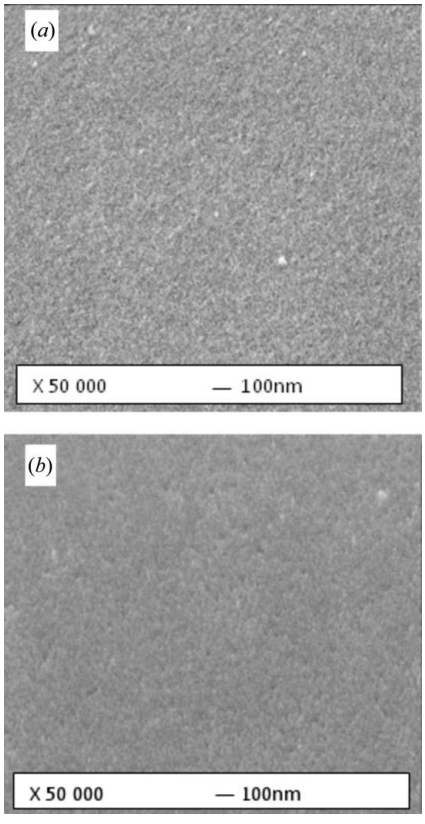

Figure 7
FE-SEM images of TiO_2 thin films deposited on (110)-oriented substrates: (*a*) STO at 873 K and (*b*) MgO at 973 K.

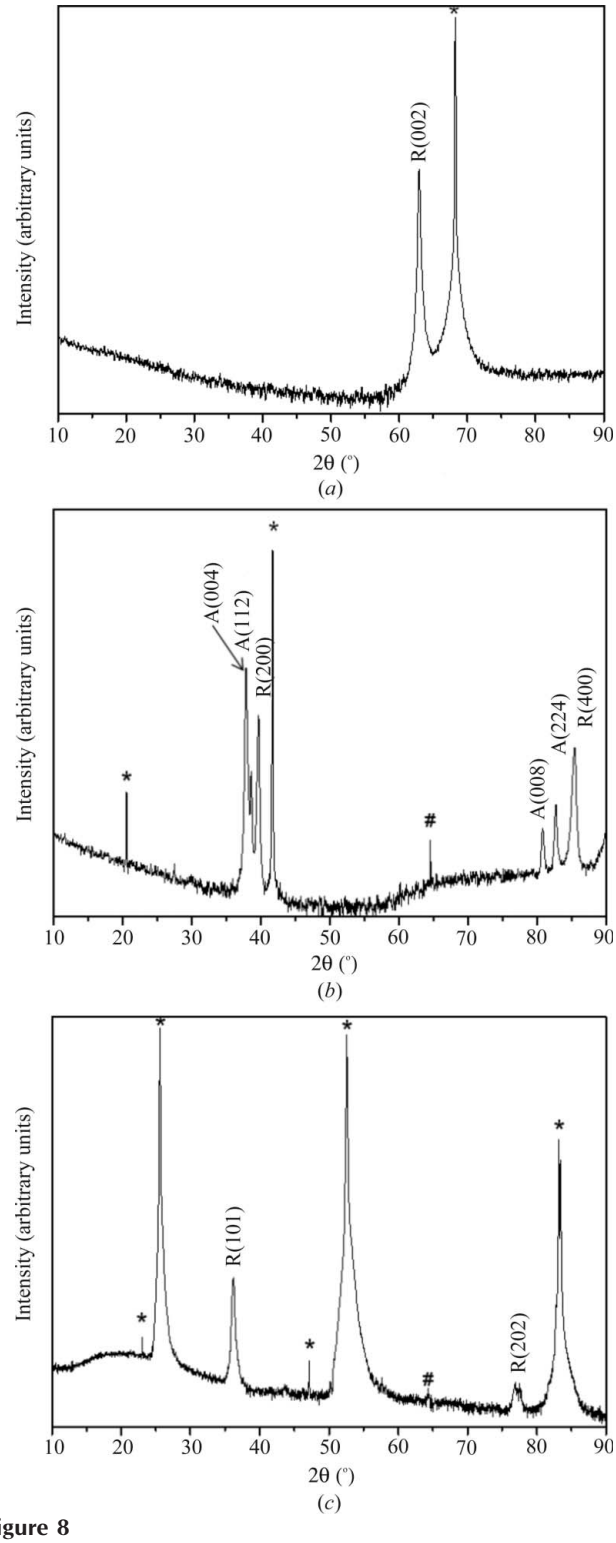

Figure 8
θ–2θ XRD patterns of the thin films deposited at 973 K on (*a*) *M*- (*b*) *C*- and (*c*) *R*-sapphire substrates. Diffraction peak labels A and R denote the anatase and rutile phases, respectively. The peaks marked with a star (⋆) or a hash sign (#) correspond to substrates and the sample holder, respectively. Note the logarithmic intensity scale.

pattern (not shown) revealed that the film was epitaxied, with four 90°-spaced peaks reflecting the fourfold symmetry of *c*-axis-oriented rutile. One of these peaks appears at the same azimuth as the $01\bar{1}2$ peak of sapphire, leading to the epitaxial relationships

$$(001)_{\rm rutile}//(10\bar{1}0)_{\rm sapphire} \text{ with } \langle 100\rangle_{\rm rutile}//[100]_{\rm sapphire} \text{ and } [001]_{\rm sapphire}. \quad (7)$$

The misfit between $a_{\rm rutile}$ and $a_{\rm sapphire}$ is $\delta = -3.5\%$, while that between $a_{\rm rutile}$ and $c_{\rm sapphire}$ (referring to one-third of the sapphire *c* axis) is $\delta = +6\%$, quite reasonable values that agree with the observation of epitaxial growth.

Note that the adjusted values of 2θ (36.15°, $\Delta\omega = 1.33°$) and χ (32.38°) associated with the 101 reflection of rutile are close to the expected ones, suggesting that the unit cell is not significantly distorted. In order to confirm this assumption, θ–2θ scans were performed in asymmetric mode. The {202} planes were chosen on the basis of geometric constraints. The $(\omega_1 - \omega_2)$ difference leads to a *c*/*a* ratio of 0.636, and, as $c_{\rm rutile}$ = 2.952 Å (bulk value: 2.959 Å) from the θ–2θ scan, then $a_{\rm rutile}$ = 4.585 Å (bulk value: 4.593 Å). The two unit-cell constants of the film are both slightly lower than those of the bulk (by about 0.2%), ruling out a strain effect.

3.3.2. TiO_2 films on *C*-plane sapphire. The θ–2θ scan of the film grown at 973 K (Fig. 8*b*) shows, in addition to the substrate 0006 reflection, two sets of peaks attributed unambiguously to 004 anatase, 112 anatase (weak), 200 rutile and their first harmonic. All these crystallites are well aligned along the growth direction, as shown by the FWHMs of their rocking curve ($\Delta\omega$ = 1.74, 1.23 and 0.11°, respectively).

The crystallites are also in-plane aligned, as shown by the φ-scan patterns (Fig. 9). The φ scan recorded for the (101) plane of the 001-oriented anatase is displayed in Fig. 9(*a*). It exhibits 12 well defined peaks ($\Delta\varphi = 2.3°$), as a result of the combination of the fourfold axis of anatase and the threefold axis of *C*-sapphire. The azimuthal shift of these peaks with respect to the $01\bar{1}2$ peaks of the substrate (marked by arrows in Fig. 9*c*) implies that the diagonal of the (001) plane of anatase is aligned with the *a* axis of sapphire, leading to the epitaxial relations

$$(001)_{\rm Anatase}//(0001)_{\rm sapphire} \text{ and } \langle 110\rangle_{\rm Anatase}//\langle 100\rangle_{\rm sapphire}. \quad (8)$$

The corresponding misfit is $\delta = +12\%$.

The φ scan recorded for the (101) plane of the 112-oriented anatase is displayed in Fig. 9(*b*). It shows six peaks ($\Delta\varphi = 3.3°$), 60°-spaced. Three of them appear at the same azimuth as the $01\bar{1}2$ peaks of the substrate, implying that the $[11\bar{1}]$ direction of anatase is aligned with the *a* and *b* axes of the substrate. The three other peaks, shifted by 180°, are deduced by symmetry:

$$(112)_{\rm anatase}//(0001)_{\rm sapphire} \text{ and } [11\bar{1}]_{\rm anatase}//\langle 100\rangle_{\rm sapphire}. \quad (9)$$

The interface plane (112) has a rectangular mesh defined by the directions $[\bar{1}10]$ and $[11\bar{1}]$ with the corresponding constants 5.353 and 5.458 Å. The misfit with sapphire is even worse ($\delta = +15\%$) than in the previous case. Note that six very weak peaks, shifted by 30° with respect to the principal ones, were observed for some films grown at 873 K. They reflect the presence of a very small amount, in this case, of in-plane-oriented crystallites with $[11\bar{1}]_{\rm anatase}//[\bar{1}10]_{\rm sapphire}$.

The φ scan recorded for the (110) plane of the 100-oriented rutile is displayed in Fig. 9(*c*). Again six peaks are observed,

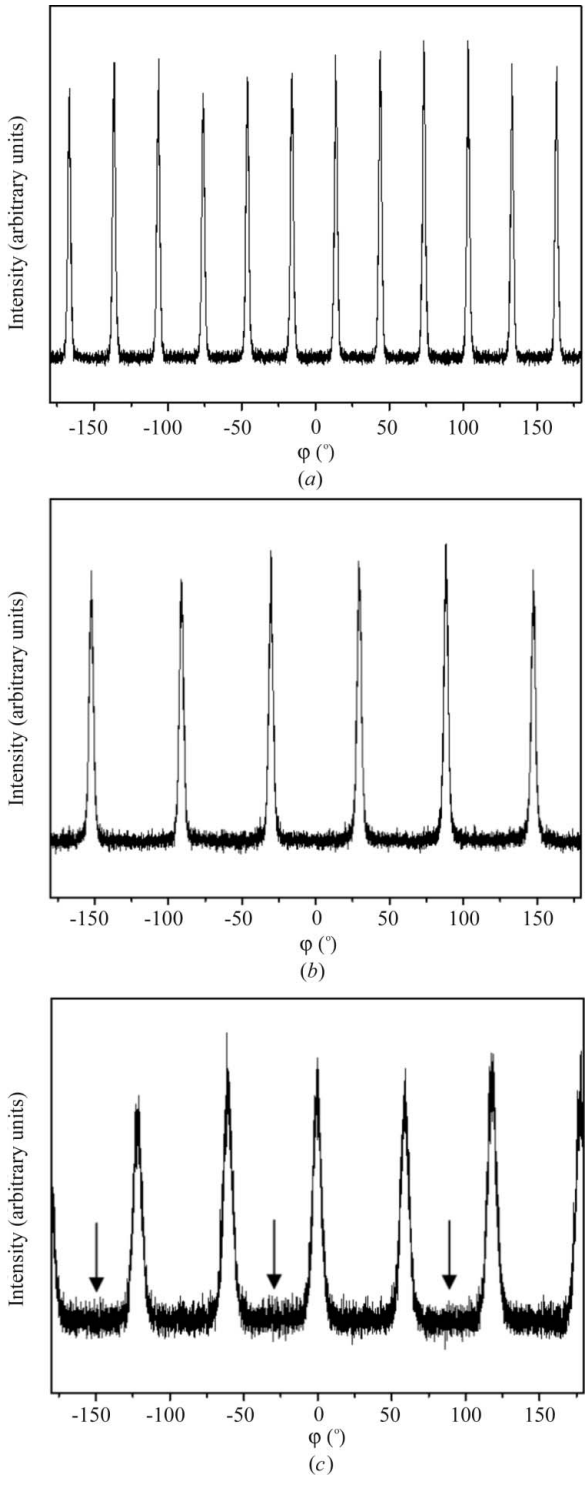

Figure 9
φ scan of a TiO_2 thin film on *C*-sapphire deposited at 973 K for (*a*) the (101) plane of the 001-oriented anatase, (*b*) the (101) plane of the 112-oriented anatase and (*c*) the (110) plane of the 100-oriented rutile. Arrows mark the azimuthal positions of the $01\bar{1}2$ substrate reflections.

from symmetry considerations, but they are significantly broader than in the previous case ($\Delta\varphi = 6^\circ$). Their azimuth with respect to substrate peaks shows that the *c* axis of the rutile crystallites lies at 30° from the *a* axis of the substrate; then

$$(100)_{\rm rutile}//(0001)_{\rm sapphire} \text{ and } [001]_{\rm rutile}//[120]_{\rm sapphire},$$
$$i.e.\ [010]_{\rm rutile}//[100]_{\rm sapphire}. \quad (10)$$

The misfit is small along the *b* axis of rutile, $\delta = -3.5\%$, but as high as -28% along the $c_{\rm rutile}$ axis; however, it is worth noting that three times the substrate mesh fits two times the rutile *c* axis within 7%. Then this orientation could be stabilized, at least to some extent, by an NCSL mechanism (Kwang *et al.*, 1980).

Note that the φ broadening is in agreement with the model proposed by Sbai *et al.* (2007), based on the competition of the above in-plane relation and an alternative very close one, for which $[001]_{\rm rutile}//[1\bar{1}0]_{\rm sapphire}$, deviating from the first orientation by 2.3°.

The influence of deposition temperature was studied in the 773–973 K range. The results are essentially the same for all samples, with some decrease of the mosaicity when deposition temperature increased. Some change of the distribution of the 004 anatase, 112 anatase and 200 rutile relative volumes was also observed, as shown on Fig. 10. As expected, the rutile volumic fraction increases sharply at 973 K at the expense of 112 anatase (but not 004 anatase, which appears to be more efficiently stabilized).

3.3.3. TiO_2 films on *R*-plane sapphire. Apart from the substrate peaks, the θ–2θ scan (Fig. 8*c*) shows only two peaks attributed to the rutile 101 and 202 reflections, giving unambiguously the film growth orientation. The rocking curve recorded around the 101 peak has $\Delta\omega = 1.38^\circ$. The φ scan recorded for the (002) plane of the 101-oriented rutile showed only one peak ($\Delta\varphi = 1.84^\circ$) at 180° from the (0006) reflection of the substrate (not shown), implying the following relations:

$$(101)_{\rm rutile}//(1\bar{1}02)_{\rm sapphire} \text{ and } [010]_{\rm rutile}//[100]_{\rm sapphire}$$
$$\text{and } [\bar{1}01]_{\rm rutile}//[\bar{1}\bar{2}1]_{\rm sapphire}. \quad (11)$$

As seen in Fig. 11, the rectangular mesh of TiO_2 (4.59 × 5.46 Å) fits reasonably the substrate surface mesh [4.76 × (2× 5.06 Å)] with $\delta = -3.6$ and 7.9%, respectively. Moreover a very good fit is observed at the atomic scale as both the metallic and the oxygen networks closely coincide. Note that both the substrate and the film structure are asymmetric in the interface plane, explaining the fact that in this case no twinning occurs.

3.3.4. Film morphology. Fig. 12 displays SEM secondary electron images for TiO_2 films grown on *M*-, *C*- and *R*-sapphire at 973 K. All samples presented a homogeneous surface, composed by very small grains. The smallest grains were obtained on *M*-sapphire, while on *R*-sapphire a more jagged surface was observed. This difference can be understood in the context of growth dynamics. Indeed, it is established that the {110} surfaces of rutile have the lowest surface energy and consequently tend to develop faster (Ramamoorthy *et al.*, 1994). This will favor a small-grained fiber texture for (100) rutile films, for which the {110} facets are perpendicular to the substrate. Conversely, in the case of (101) rutile, for which the fast-growing facets develop at 67.5° from the substrate, a rough surface can be expected. This model fully explains the detail of the microstructure recently reported by Yeh *et al.* (2010).

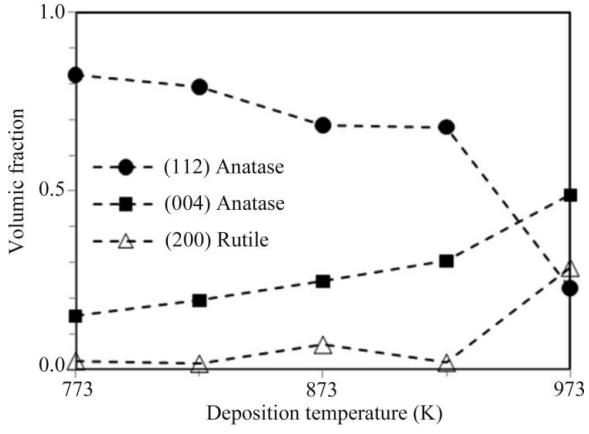

Figure 10
Distribution as a function of deposition temperature of (001)- and (112)-oriented anatase and (100)-oriented rutile crystallites for TiO_2 films grown on *C*-plane sapphire.

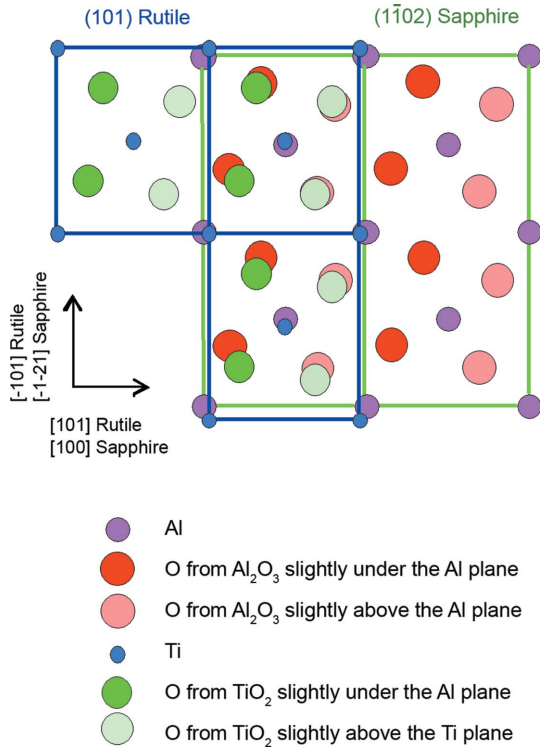

Figure 11
A sketch of the atomic coincidences at the interface between (101) rutile and (1$\bar{1}$02) sapphire. For clarity, three unit cells of rutile and two of sapphire are drawn and the atom sizes are not scaled.

4. Discussion and conclusions

Titanium oxide is among the most studied materials worldwide, because of its extremely promising applications, and there are obviously a lot of studies related to TiO_2 thin films grown by various methods, including PLD. However, because the existing literature data cover a broad range of different methods of deposition, different conditions, different substrates *etc.*, we have carried out a systematic study, choosing a single technique of film growth (pulsed laser deposition) and a limited range of temperature, but a wide variety of (single-crystal) oxide substrates, including $LaAlO_3$, two different orientations of $SrTiO_3$ and MgO, and three orientations of sapphire. Additionally, the effect of deposition temperature was checked in selected examples, owing to the existence of several allotropes of TiO_2 (mainly anatase and rutile).

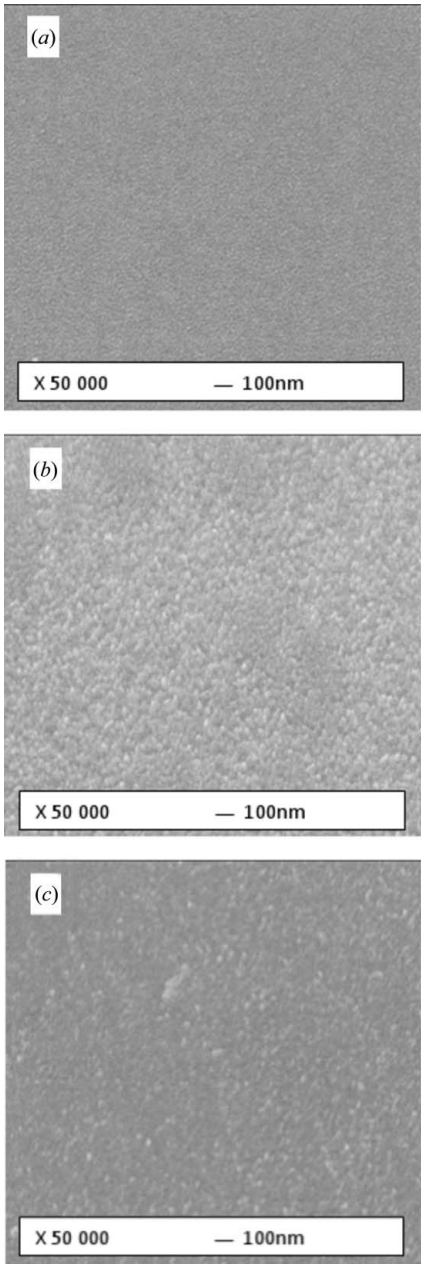

Figure 12
FE-SEM images of TiO_2 thin films deposited at 973 K on (*a*) *M*- (*b*) *C*- and (*c*) *R*-sapphire substrates.

Table 1
Summary of results obtained in the present work on the different substrates.

All films are epitaxial. Unless stated otherwise, the deposition temperature is 873 K.

	Phase	
Substrate	Rutile	Anatase
STO(100)	–	(001)
LAO(100)	–	(001)
MgO(100)		
773 K	–	(100)
873 K	–	(100)
973 K	(110)	(100)
STO(110)	–	(102)
MgO(110)		
773 K	–	(110) + (102)
873 K	–	(102)
973 K	(110)	(102)
M-Sapphire	(001)	–
C-Sapphire, 773–973 K	(100)	(001) + (112)
R-sapphire	(101)	–

Epitaxial anatase and rutile phases were selectively obtained and our results are summarized in Table 1. The crystalline orientation and quality strongly depend on the substrate nature, as well as its orientation. (100)LAO and (100)STO substrates provided (001) anatase films presenting very good crystalline quality. For the same deposition temperature of 873 K, (100)- and (110)MgO substrates gave oriented but more misaligned microstructures, very probably as a result of the high misfit, of (100) and (102) anatase, respectively. In contrast on (110)STO, high-quality epitaxial (102) anatase was observed. On *R*- and *M*-sapphire substrates, an epitaxial growth of rutile was obtained with (101) and (001) orientations, respectively. In contrast, on *C*-sapphire three types of crystallites, all epitaxied, coexist: (001) anatase, (112) anatase and (100) rutile. These results show that the film–substrate interactions are able to promote either the rutile or/and the anatase allotropes, quite independently of the growth temperature. Nevertheless, increasing the temperature tends to favor the rutile allotrope, as clearly shown, for instance, in the examples of films grown on (100) and (110) MgO or *C*-plane sapphire. This result is obviously in agreement with the thermodynamics of the anatase–rutile equilibrium. However, it is worth noting that this equilibrium can also be affected by doping effects that change the temperature transition (Rao *et al.*, 1959; Gennari & Pasquevich, 1998; Rodriguez-Talavera *et al.*, 1997).

Table 2 summarizes some examples of literature data and shows that our results are in general agreement with them: this is the case on (100)- and (110)STO, (100)MgO, and (100)LAO, as well as on *M*- and *R*-sapphire, although polycrystalline samples were reported in some examples. The main differences concern, for instance, the (102) anatase growth on (110) MgO; only a few reports on the growth of TiO_2 on this

Table 2
Some examples of literature data on TiO_2 thin films grown on substrates.

Unless stated otherwise, films are epitaxial. A and R refer to anatase and rutile phases, respectively. Poly: polycrystalline without orientation; PLD: pulsed laser deposition; REBE: reactive electron beam evaporation; IBSD: ion beam sputter deposition; Sputt: direct current magnetron sputtering; ALD: atomic layer deposition; MBE: molecular beam epitaxy.

(*a*) (100)-oriented substrates.

(100)STO	(100)LAO	(100)MgO	Method	References
A(001)	A(001)	A(100)	PLD	Yamamoto *et al.* (2001)
A(001)	A(001)	–	REBE	Lotnyk *et al.* (2007)
A(001) + weak textured R(111)	A(001)	–	PLD	Kennedy & Stampe (2003)
–	A(001)	–	PLD	Kitazawa *et al.* (2006), Sakama *et al.* (2006), Park *et al.* (2002)
–	A(001)	–	Sputt	Singh *et al.* (2008)
–	–	A(100)	IBSD	Morris Hotsenpiller *et al.* (1996)
–	–	A(100)	ALD	Schuisky *et al.* (2002), Mitchell *et al.* (2005)
–	–	Partially oriented A(001) + weak R(200) and R(111)	PLD	Garapon *et al.* (1996)

(*b*) (110)-oriented substrates.

(110)STO	(110)MgO	Method	References
Poly mixed A+R	Poly mixed A+R	PLD	Yamamoto *et al.* (2001)
A(012)	–	REBE	Lotnyk *et al.* (2007)
A(102)	–	PLD	Kennedy & Stampe (2003)
–	R(110)	IBSD	Morris Hotsenpiller *et al.* (1996)

(*c*) Sapphire substrates.

M-Sapphire	*C*- Sapphire	*R*-Sapphire	Method	References
R(101)	R(100)	R(101)	PLD	Yamamoto *et al.* (2001)
R(001)	R(100)	–	PLD	Yamamoto *et al.* (2002)
R(001)	R(100)	R(101)	IBSD	Morris Hotsenpiller *et al.* (1996)
–	R(100) + textured A(001)	–	PLD	Yamaki *et al.* (2002)
–	A(001) + R(100)	–	PLD	Kitazawa *et al.* (2006), Sbai *et al.* (2007)
–	R(100)	–	PLD	Xin *et al.* (2006)
–	R(100)	–	Sputt	Singh *et al.* (2008)
–	–	R(101)	MBE	Engel-Herbert *et al.* (2009)
–	–	R(101)	ALD	Schuisky *et al.* (2002)

substrate are available, and our finding of (102) anatase is unique, probably because it is impossible to assess this orientation without the help of pole figures. Morris Hotsenpiller *et al.* (1996) reported a (110) rutile growth (also present in our study for the highest temperature), but one can guess they missed the possible presence of (102) anatase for the above-mentioned reason. Also, on *C*-sapphire, we observed very reproducibly the previously unreported epitaxial growth of (112) anatase crystallites, together with (001) anatase and (100) rutile. This means that, additionally to the primary effect, namely the substrate structure-induced growth, secondary effects related to deposition conditions can be invoked: for instance by direct current magnetron sputtering, Singh *et al.* (2008) observed only (100) rutile on *C*-sapphire at a deposition temperature of 923 K. More unexpectedly, Yamamoto *et al.* (2001) obtained this unique orientation by PLD, but it is worth noting that they worked with a different laser wavelength and a fluence lower than ours by an order of magnitude.

Another illustration of the effect of experimental conditions is given by the results of Yamamoto *et al.* (2001): using a KrF laser, they obtained, like us, (001) rutile on *M*-sapphire, while in their first report they obtained, in contrast, (101) rutile by the use of a second harmonic Nd/YAG laser. Also note that Kitazawa *et al.* (2006) reported a mixture of (001) anatase + (100) rutile for PLD films grown on *C*-sapphire and found, for the same deposition temperature, an increase of the rutile/anatase ratio when increasing the fluence. Incidentally, at low pressure (10 Pa), they observed an unidentified peak, which could in fact be assigned to (112) anatase, as in this report.

In summary, we succeeded in the epitaxial growth of all these films, evidenced by an accurate X-ray diffraction study, including rocking curves and φ scans. We have shown that we can control orientations as diverse as (001), (102), (100), (110) and (112) anatase and (110), (001), (100) and (101) rutile. In some cases, where several phases and/or orientations coexist, we evaluated their volumic fraction, a parameter that would be of importance for further studies. Meanwhile, a major target of this study was the accurate determination of epitaxial relationships between the film and the substrate, the comprehension of what happens at the interface, and the building of interfacial models. The example of TiO_2 growth on *R*-plane sapphire is of special interest in this context: remember that this substrate is commonly chosen for the growth of (100)-oriented perovskites (Rousseau *et al.*, 2008) or perovskite-related materials (Thivet *et al.*, 1994). High-quality (101) rutile films are grown on this substrate, even at a temperature as low as 873 K. For comparison, at the same temperature, (001) anatase is observed on the (100)STO perovskite substrate, and even on (100)LAO (which is in fact the *R* plane of the latter material in its actual trigonal structure, but presents an arrangement close to the perovskite one). The preferential growth of (101) rutile on *R*-sapphire has then to be related to the structural identity of the two materials at the interface (refer to Fig. 11) and is a very illustrative example of substrate-induced structure stabilization.

The authors acknowledge the CAPES-COFECUB (project No. 644/09) for financial support, and I. Peron and J. Le Lannic for obtaining SEM images at CMEBA, University of Rennes.

References

Aarik, J., Karlis, J., Mändar, H., Uustare, T. & Sammelselg, V. (2001). *Appl. Surf. Sci.* **181**, 339–343.

Banfield, J. F., Bischoff, B. L. & Anderson, M. A. (1993). *Chem. Geol.* **110**, 211–231.

Bourdias, C. & Monceau, D. (1998). *CaRine Crystallography*. Version 3.1. Divergent S.A., Compiègne, France.

Diedold, U. (2003). *Surf. Sci. Rep.* **48**, 53–229.

Engel-Herbert, R., Jalan, B., Cagnon, J. & Stemmer, S. (2009). *J. Cryst. Growth*, **312**, 149–153.

Garapon, C., Champeaux, C., Mugnier, J., Panczer, G., Marchet, P., Catherinot, A. & Jacquier, B. (1996). *Appl. Surf. Sci.* **96–98**, 836–841.

Gennari, F. C. & Pasquevich, D. M. (1998). *J. Mater. Sci.* **33**, 1571–1578.

Heikkilä, M., Puukilainen, E., Ritala, M. & Leskelä, M. (2009). *J. Photochem. Photobiol. B*, **204**, 200–208.

Heo, C. H., Lee, S.-B. & Boo, J.-H. (2005). *Thin Solid Films*, **475**(1–2), 183–188.

Hesse, D. & Bethge, H. (1981). *J. Cryst. Growth*, **52**, 875–882.

Kennedy, R. J. & Stampe, P. A. (2003). *J. Cryst. Growth*, **252**, 333–342.

Kim, D.-J., Kang, J.-Y. & Kim, K.-S. (2010). *Adv. Powder Technol.* **21**, 136–140.

King, D. M., Liang, X., Zhou, Y., Carney, C. S., Hakim, L. F., Li, P. & Weimer, A. W. (2008). *Powder Technol.* **183**, 356–363.

Kitazawa, S.-I., Choi, Y., Yamamoto, S. & Yamaki, T. (2006). *Thin Solid Films*, **515**, 1901–1904.

Kwang, M., Laughin, D. E. & Bernstein, I. M. (1980). *Acta Metall.* **28**, 621–632.

Lotnyk, A., Senz, S. & Hesse, D. (2007). *Thin Solid Films*, **515**, 3439–3447.

Meng, F., Song, X. & Sun, Z. (2009). *Vacuum*, **83**, 1147–1151.

Mitchell, D. R. G., Attard, D. J. & Triani, G. (2005). *J. Cryst. Growth*, **285**, 208–214.

Morris Hotsenpiller, P. A., Wilson, G. A., Roshko, A., Rothman, J. B. & Rohrer, G. S. (1996). *J. Cryst. Growth*, **166**, 779–785.

Park, B. H., Huang, J. Y., Li, L. S. & Jia, Q. X. (2002). *Appl. Phys. Lett.* **80**, 1174–1176.

Ramamoorthy, M., Vanderbilt, D. & King-Smith, R. D. (1994). *Phys. Rev. B*, **49**, 16721–16727.

Rao, C. N. R., Turner, A. & Honig, J. M. (1959). *J. Phys. Chem. Solids*, **11**, 173–175.

Rodriguez-Talavera, R., Vargas, S., Arroyo-Murillo, R., Montiel-Campos, R. & Haro-Poniatowski, E. (1997). *J. Mater. Res.* **12**, 439–443.

Rousseau, A., Laur, V., Députier, S., Bouquet, V., Guilloux-Viry, M., Tanné, G., Laurent, P., Huret, F. & Perrin, A. (2008). *Thin Solid Films*, **516**, 4882–4888.

Sakama, H., Osada, G., Tsukamoto, M., Tanokura, A. & Ichikawa, N. (2006). *Thin Solid Films*, **515**, 535–539.

Sbai, N., Perrière, J., Seiler, W. & Million, E. (2007). *Surf. Sci.* **601**, 5649–5658.

Schuisky, M., Kukli, K., Aarik, J., Lu, J. & Harsta, A. (2002). *J. Cryst. Growth*, **235**, 293–299.

Shannon, R. D. & Pask, J. A. (1965). *J. Am. Ceram. Soc.* **48**, 391–398.

Singh, P., Kumar, A. & Kaur, D. (2008). *Physica B*, **403**, 3769–3773.

Sobczyk-Guzenda, A., Gazicki-Lipman, M., Szymanowski, H., Kowalski, J., Wojciechowski, P., Halamus, T. & Tracz, A. (2009). *Thin Solid Films*, **517**, 5409–5414.

Sun, H., Wang, C., Pang, S., Li, X., Tao, Y., Tang, H. & Liu, M. (2008). *J. Non-Cryst. Solids*, **354**, 1440–1443.

Thivet, C., Guilloux-Viry, M., Padiou, J., Perrin, A., Dousselin, G., Pellan, Y. & Sergent, M. (1994). *Physica C*, **235–240**, 665–666.

Walczak, M., Papadopoulou, E. L., Sanz, M., Manousaki, A., Marco, J. F. & Castillejo, M. (2009). *Appl. Surf. Sci.* **255**, 5267–5270.

Xin, Y., Han, K., Stampe, P. A. & Kennedy, R. J. (2006). *J. Cryst. Growth*, **290**, 459–465.

Yamaki, T., Sumita, T., Yamamoto, S. & Miyashita, A. (2002). *J. Cryst. Growth*, **237–239**, 574–579.

Yamamoto, S., Sumita, T., Sugiharuto, Miyashita, A. & Naramoto, H. (2001). *Thin Solid Films*, **401**, 88–93.

Yamamoto, S., Sumita, T., Yamaki, T., Miyashita, A. & Naramoto, H. (2002). *J. Cryst. Growth*, **237–239**, 569–573.

Yeh, C. N., Chen, Y. M., Chen, C. A., Huang, Y. S., Tsai, D. S. & Tiong, K. K. (2010). *Thin Solid Films*, **518**, 4121–4129.

Zhao, L. & Lian, J.-S. (2007). *Trans. Nonferrous Met. Soc. China*, **17**, 772–776.